Available online at www.sciencedirect.com
ScienceDirect
Physica B 394 (2007) 122–126
PHYSICA B
www.elsevier.com/locate/physb

Magnetic properties of Mn-doped cubic silicon carbide

S.B. Ma, Y.P. Sun*, B.C. Zhao, P. Tong, X.B. Zhu, W.H. Song

Key Laboratory of Materials Physics, Institute of Solid State Physics, Chinese Academy of Sciences, Hefei 230031, People's Republic of China

Received 16 January 2007; received in revised form 13 February 2007; accepted 17 February 2007

Abstract

Bulk polycrystalline $Si_{1-x}Mn_xC$ ($0 \leqslant x \leqslant 0.1$) samples were prepared by the solid-state reaction method. Their structural and magnetic properties had been investigated. Powder X-ray diffraction analysis demonstrates that the appropriate Mn doping does not change the crystal structure of cubic silicon carbide (3C-SiC). Magnetic studies reveal that the ferromagnetism can be developed when Mn substitution is as low as $x = 0.01$. The Curie temperature (T_C) increases monotonously with increasing Mn-doped content up to $x = 0.05$, and then almost keeps constant as x further increases. The effective magnetic moments are $2.05\mu_B$/Mn, $1.19\mu_B$/Mn, $0.90\mu_B$/Mn, and $0.89\mu_B$/Mn for the samples with $x = 0.01$, 0.03, 0.05, and 0.1, respectively.

PACS: 72.25.Dc; 75.50.Pp; 75.50.Gg; 75.60.Ej

Keywords: Diluted magnetic semiconductors; Mn doping; Cubic silicon carbide; Ferromagnetism

1. Introduction

Diluted magnetic semiconductors (DMSs) have been a focus of intensive studies due to the possibility of integrating charge and spin degree of freedom in a single material [1]. III–V compounds doped with transition metal is the most widely studied material of this class, such as $Ga_{1-x}Mn_xAs$, in which ferromagnetic (FM) ordering is found with the Curie temperature (T_C) up to 170 K and has been successfully utilized as spin-polarized devices [2–4]. Moreover, room temperature ferromagnetism has been found in Mn-doped $CdGeP_2$ [5], $ZnGeP_2$ [6–8] and $ZnGeAs_2$ [9] DMSs. The group-IV-based DMSs materials have been earnestly expected to the favorable category with T_C above room temperature due to their compatibility with conventional integrated circuits. Recently, it is very excited due to the discovery of ferromagnetism in $Ge_{1-x}Mn_x$ ($x = 0.05$) epitaxial thin films with T_C up to 110 K [10]. In addition, the ferromagnetism formed in the Mn-doped silicon system has also been reported [11,12]. Furthermore, recent theoretical prediction by Dietl et al. [13] suggests that T_C is related to the magnitude of the band gap of the semiconductor, such as (Ga,Mn)N and (Zn,Mn)O were predicted to have T_C values above room temperature for sufficiently high acceptor doping levels.

Compared with the extensive study on the conventional DMSs, very little attention has been paid to the potential DMSs behavior of doped SiC so far. In the microelectronics realm, silicon carbide, with its wide band gap (2.4 eV for the 3C polytype), excellent transport properties and doped ability, is regarded as a promising substitute for silicon, especially in high-power, high-temperature, and high-frequency devices [14,15]. The large band gap of SiC implies that the acceptor and/or donor levels might be far away from their respective valence and conduction band edges to ensure a high enough density of itinerant carriers for carrier mediated ferromagnetism. The SiC-based DMS films prepared by transition metal ions implanted method exhibit ferromagnetism with T_C approximately 50 K for Ni, 250 K for Mn, and 270 K for Fe [16,17].

In this paper, we report the structural and magnetic properties of a series of $Si_{1-x}Mn_xC$ ($x = 0$, 0.01, 0.03, 0.05, and 0.1) bulk polycrystalline samples synthesized by

*Corresponding author. Tel.: +86 551 559 2757; fax: +86 551 559 1434.
E-mail address: ypsun@issp.ac.cn (Y.P. Sun).

0921-4526/$ - see front matter © 2007 Elsevier B.V. All rights reserved.
doi:10.1016/j.physb.2007.02.028

conventional solid-state reaction method. All doped samples show ferromagnetism and T_C increases from 205 K for $x = 0.01$ to about 250 K for the $x = 0.05$ sample.

2. Experiment

Bulk polycrystalline samples of $Si_{1-x}Mn_xC$ with nominal composition of $x = 0$, 0.01, 0.03, 0.05, and 0.1 were fabricated by conventional solid-state reaction method. High-purity manganese (99.97%), carbon (99.99%), and silicon (99.999%) powders were weighted in an appropriate ratio and homogenized in an agate pestle. At first, the homogenized mixture was pressed into pellets and loaded into a columned corundum tube with one sealed end. Secondly, the corundum tube was evacuated ($<10^{-4}$ Torr) and filled with high purity argon as protecting gas. Finally, the sealed corundum tube was loaded into a vertical furnace and sintered. The corundum tube was first heated to 1000 °C and held at this temperature for 24 h. The powder obtained was ground, palletized, and sintered at 1450 °C for 24 h, and finally, the furnace was slowly cooled down to room temperature.

The structure and phase analysis of the samples were examined by powder X-ray diffraction (XRD) using CuKα radiation at room temperature. The magnetization of the samples was measured on a Quantum Design superconducting quantum interference device magnetic property measurement system ($1.9\,K \leqslant T \leqslant 400\,K$, $0\,T \leqslant H \leqslant 7\,T$). Both the zero-field-cooled (ZFC) and field-cooled (FC) magnetization data were collected.

3. Results and discussion

Fig. 1(a) shows the powder XRD patterns of bulk $Si_{1-x}Mn_xC$ ($x = 0$, 0.01, 0.03, 0.05, and 0.1) samples. The XRD at room temperature shows that all samples are single phase with no detectable secondary phases, even the intensity in logarithmic scale. As we know, SiC has a multitude of polytypes in more than 200 different structures. The most widely used is 3C, 4H, and 6H [18]. According to the standard cards of XRD, the present samples can be indexed as cubic silicon carbide (3C-SiC) with the space group F43m. The structure parameters can be obtained by fitting the experimental spectra using the standard Rietveld technique [19]. The obtained lattice constant d increases monotonously with increasing Mn-doped content, which are listed in Table 1. This result is consistent with the fact that Mn ion has larger ionic radii than that of silicon. The conclusion can also be confirmed by the shift of the (1 1 1) peak position towards smaller angles as shown in the Fig. 1(b), implying the increase of lattice parameters. Therefore, we can conclude that the mixed phase does not exist in present samples, though support from a more accurate analysis technique is needed.

Fig. 2 plots the temperature dependence of magnetization $M(T)$ for $Si_{1-x}Mn_xC$ between 5 and 320 K under both ZFC and FC modes at 1000 Oe. Fig. 2 shows that Mn-free sample behaves as a PM feature, which is coincident with the earlier reported result [20]. For all doped samples, the $M(T)$ curves show a typical characteristic of a paramagnetic (PM) to FM phase transition. The obtained transition temperature (Curie temperature) T_C (defined as the one corresponding to the peak of dM/dT in the M vs. T curve)

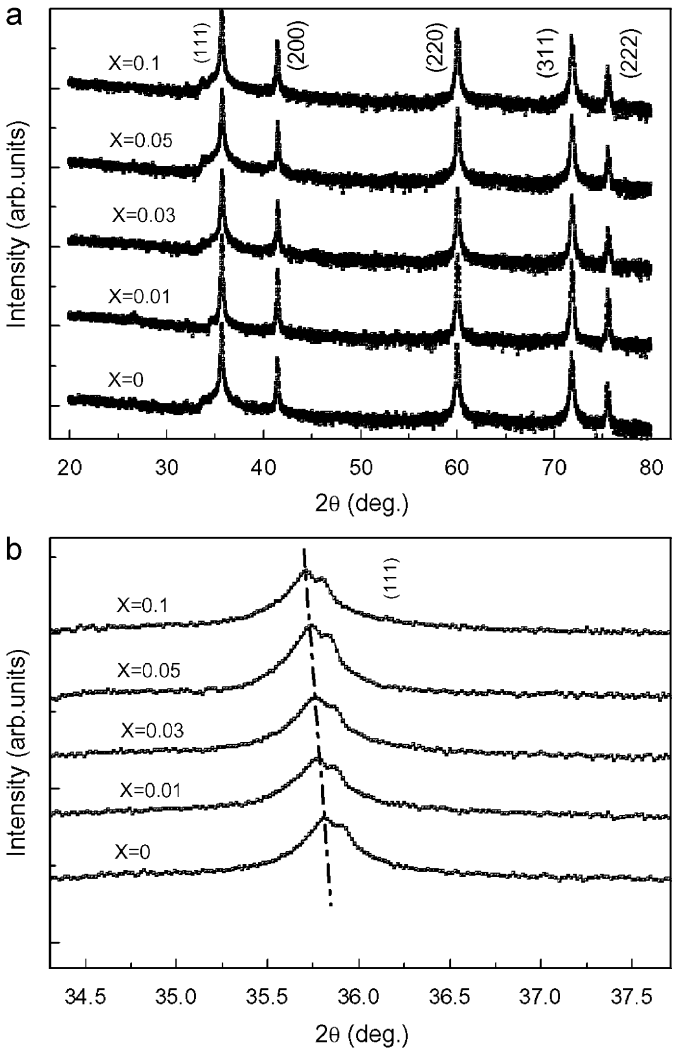

Fig. 1. (a) Powder XRD patterns for polycrystalline bulk $Si_{1-x}Mn_xC$ ($x = 0$, 0.01, 0.03, 0.05, and 0.1) samples, and (b) shows the shift of the (1 1 1) peak position. The dash dots are just guides to eye.

Table 1
Structural and magnetic parameters of $Si_{1-x}Mn_xC$ polycrystalline bulk samples

Sample	d (nm)	T_C (K)	θ (K)	μ_{eff} (μ_B)
$x = 0$	4.3596	–	–	–
$x = 0.01$	4.3607	205	112.8	2.05
$x = 0.03$	4.3612	220	153.5	1.19
$x = 0.05$	4.3619	252	260.3	0.90
$x = 0.1$	4.3628	250	238.9	0.89

From left to right, the columns indicate sample composition; lattice constant; Curie temperature; Weiss temperature; and effective magnetic moment.

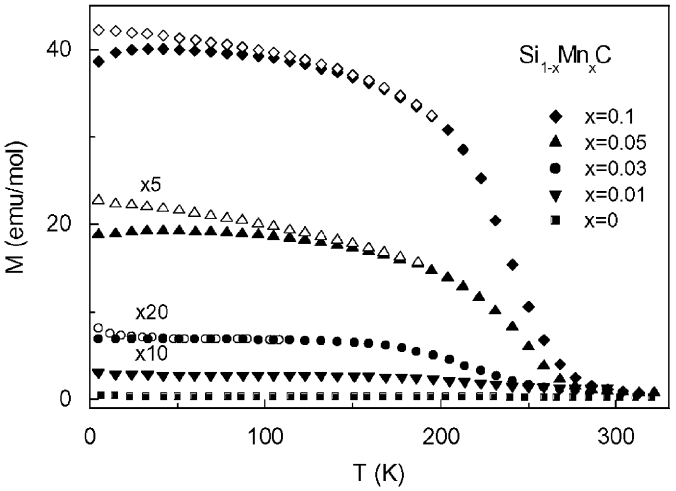

Fig. 2. Magnetization as a function of temperature for polycrystalline bulk $Si_{1-x}Mn_xC$ ($x = 0$, 0.01, 0.03, 0.05, and 0.1) samples measured at $H = 1000$ Oe under the zero-field-cooled (ZFC; filled symbol) and field-cooled (FC; open symbol) modes. The symbol $\times 5$, $\times 20$, and $\times 10$ on the plots denote the amplified times for the sake of clarity.

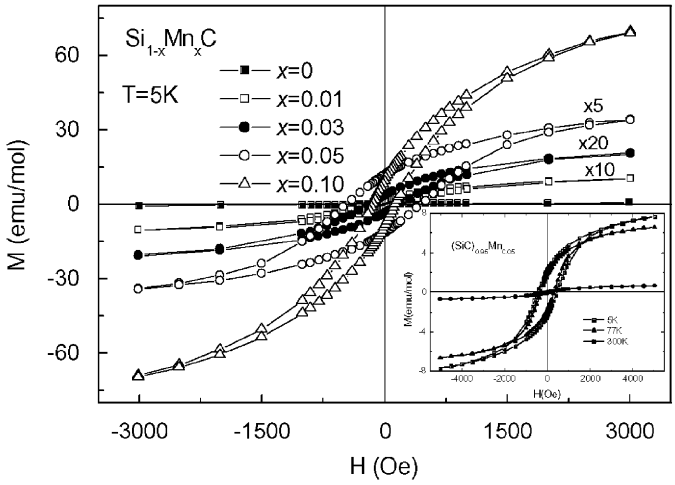

Fig. 3. Magnetic hysteresis loops at 5 K for polycrystalline bulk $Si_{1-x}Mn_xC$ ($x = 0$, 0.01, 0.03, 0.05, and 0.1) samples. The sign $\times 5$, $\times 20$, and $\times 10$ on the curves denote the amplified times for the sake of clarity. The insert is the hysteresis loops for the sample $Si_{0.95}Mn_{0.05}C$ at 5, 77, and 300 K, respectively.

is 205, 220, 252, and 250 K for the sample with $x = 0.01$, 0.03, 0.05, and 0.1, respectively. T_C increases monotonously with increasing Mn-doped concentration up to $x = 0.05$, and then T_C almost keeps constant as x further increases. As shown in Fig. 2, the FC magnetization curve is almost superposed on the ZFC curve for the $x = 0$ and 0.01 samples (for $x = 0$ and 0.01 at the FC model not shown here). No obvious difference is observed between the ZFC and FC curves. In contrast, for the heavy-doped samples with $x > 0.01$, FC $M(T)$ curves do not coincide with the ZFC $M(T)$ curves at low temperature. Moreover, the difference between the ZFC and FC magnetization increases with increasing Mn-doped concentration. Such data have been observed before in several systems and are typically interpreted in terms of the competition between antiferromagnetic (AFM) and FM interaction [21]. The result indicates that both FM and AFM interactions can be induced by Mn-doped SiC system and the competition between them varies with increasing Mn-doped concentration. This discrepancy between ZFC and FC magnetization is a characteristic of magnetic clusters. The detailed analysis of the ferromagnetism existing in present samples will be shown below. The resulting AFM phase in the sample may be related to the inhomogeneity of Mn distribution. Similar spatial fluctuation of the Mn content was reported in Mn-doped ZnTe by the neutron scattering experiment [22]. From the above analysis, we may conclude that the Mn ions in the doping samples do not substitute Si ions uniformly but fluctuate spatially.

The magnetic hysteresis loop $M(H)$ curves of all studied samples at 5 K are shown in Fig. 3. No hysteresis was observed for Mn-free sample, indicating the sample is predominantly PM, which is consistent with the result obtained from the curve of $M(T)$. On the other hand, a clear hysteresis curve with coercive field, $H_c \sim 180$, 188, 460, and 140 Oe, was obtained for the sample with $x = 0.01$, 0.03, 0.05, and 0.1, respectively, indicating the introduction of ferromagnetism due to Mn doping. Obviously, the coercive field increases first with the Mn concentration and decreases for high Mn concentration ($x > 0.05$). It is suggested that the coercive field increase attributes to the increase of Mn ions incorporated in lattice of silicon, and these Mn ions formed FM coupling. As Mn concentration is over certain critical value, the nearest Mn ions, due to direct interaction, formed AFM coupling, resulting in deduction of coercive field [7,11]. The saturation magnetization M_s increases sharply in an ordered level as Mn-doped concentration over 5% and the magnetization is not saturation up to 4500 Oe for the heavy doping samples with $x > 0.03$. The $M(H)$ measurement has also been performed at 5, 77, and 300 K. As an example, the $M(H)$ curves at 5, 77, and 300 K for the sample with $x = 0.05$ are displayed in the inset of Fig. 3. The coercive field is 460 and 310 Oe at 5 and 77 K, respectively. From the insert, we found that no room temperature ferromagnetism is observed and the magnetization is not saturation up to 5000 Oe at 5 and 77 K. In addition, the slightly Mn-doped sample ($x = 0.01$) showed PM-like in Fig. 2. In this scenario, it is assumed that the substituted Mn ions are separated to order, resulting in a PM state. For a higher Mn concentration, long-range ordering sets up, but magnetization did not saturate even at high magnetic fields, which may contribute to the presence of PM-like and FM Mn regions. Similar results were obtained in Mn-doped Ge and $ZnGeP_2$ [7,8].

In order to further understand the magnetic properties of the Mn-doped 3C-SiC, the temperature dependence of the inverse magnetic susceptibility ($\chi^{-1} = H/M$) for the doping samples is plotted in Fig. 4. It can be seen that the experimental curves in the PM phase above T_C can be well described by the Curie–Weiss law, i.e., $\chi = C/(T-\Theta)$,

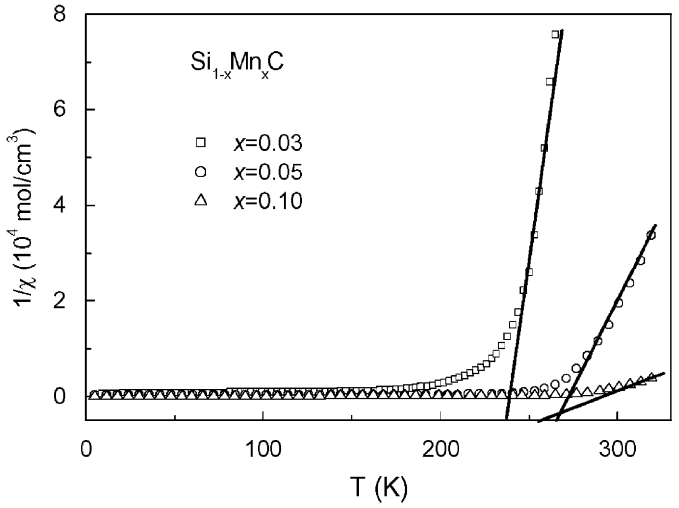

Fig. 4. The temperature dependence of the inverse of the magnetic susceptibility for $Si_{1-x}Mn_xC$ samples with $x = 0.03$, 0.05, and 0.1. The solid line is the fitting curve according to the Curie–Weiss law.

where C is the Curie constant, and Θ is the Weiss temperature. The effective magnetic moment μ_{eff} obtained from the fitting is $2.05\mu_B$/Mn, $1.19\mu_B$/Mn, $0.9\mu_B$/Mn, and $0.89\mu_B$/Mn for the samples with $x = 0.01$, 0.03, 0.05, and 0.1, respectively. μ_{eff} decreases sharply as Mn-doped content x increases from 0.01 to 0.05, μ_{eff} for the $x = 0.1$ sample is almost the same with that of the $x = 0.05$ sample. The effective magnetic moment decrease with increasing Mn concentration is strong evidence that the AFM coupling overcomes FM interaction due to the closer spacing of the Mn ions. Similar result was also obtained in Mn-ion implanted Si [11].

In the following, we further discuss the magnetism for the SiC-based DMSs doped with Mn. Several models have recently been suggested that Mn-doped 3C-SiC DMSs shows a stable ferromagnetism. Magnetic moment is 1.0 μ_B/Mn using the linearized full-potential muffin-tin orbital (MTO) method [18,23–25]. From our experimental results, magnetic moment in Mn-doped 3C-SiC DMSs is $0.9\mu_B$/Mn with 5% Mn concentration, which is lightly less than the theoretical value obtained by the linearized full-potential MTO method. It is intelligible when spatial fluctuation of the Mn concentration, which is mentioned above, is taken into account. In comparison with the other group IV [10,26] and III–V-based DMSs [27–32], the magnetic moment is very small for Mn-doped SiC, indicating a significantly different magnetic interaction of Mn impurity than in the other hosts. According to the linearized full-potential MTO model, the Mn-d level and the C dangling bond are strongly coupled because of their proximity in energy and induce a large crystal-field splitting that suppresses the spin-polarization. As a result, manganese is in a low-spin state, which has only $1\mu_B$/Mn [18].

Of great concern when measuring magnetic properties of SiC-based DMSs is the presence of the second phases. Pure SiC does not have a net magnetic moment, resulting in paramagnetism. Metallic Mn is AFM, with a Néel temperature of 100 K [33]. In addition, in all Si–Mn or Mn–C compounds, only Mn_4Si_7 and MnSi are of FM and their Curie temperature is about 30 and 47 K, respectively [34,35]. We have carefully searched for Si–Mn or Mn–C alloying secondary phase such as MnC, MnSi, Mn_5Si_3, Mn_4Si_7, and Mn_3Si; however, no obvious secondary phase was found from Fig. 1(a), even in logarithmically scaled XRD patterns. Thus, the observed magnetic properties in all investigated samples with about 250 K Curie temperature appear to exclude the possibility of the second phase effect. However, further investigation in the structural properties is needed.

4. Conclusion

In summary, we have prepared bulk $Si_{1-x}Mn_xC$ DMSs with $x = 0$, 0.01, 0.03, 0.05, and 0.1 using solid-state reaction method. The prepared samples are of 3C-SiC cubic structure and no obvious secondary phase was observed from the XRD patterns. The lattice constant increases with increasing Mn concentration x. All doping samples undergo a PM–FM transition with T_C from 205 to 250 K. The effective magnetic moments are $2.05\mu_B$/Mn, $1.19\mu_B$/Mn, $0.9\mu_B$/Mn, and $0.89\mu_B$/Mn for the samples with $x = 0.01$, 0.03, 0.05, and 0.1, respectively. A threshold concentration for Mn doping 3C-SiC exists. These results have considerable implications for the fundamental understanding of FM in DMS materials and for SiC-based device applications.

Acknowledgments

This work was supported by the National Key Research under Contract No. 001CB610604, and the National Nature Science Foundation of China under Contract No. 10474100, 10374033 and Director's Fund of Hefei Institutes of Physical Science, Chinese Academy of Sciences.

References

[1] G.A. Prinz, Science 282 (1998) 1660.
[2] H. Ohno, A. Shen, F. Matsukura, A. Oiwa, A. Endo, S. Katsumoto, Y. Iye, Appl. Phys. Lett. 69 (1996) 363.
[3] Y.D. Park, B.T. Jonker, B.R. Bennett, G. Itskos, M. Furis, G. Kioseoglou, A. Petrou, Appl. Phys. Lett. 77 (2000) 3989.
[4] K.W. Edmonds, K.Y. Wang, R.P. Campion, A.C. Neumann, N.R.S. Farley, B.L. Gallagher, C.T. Foxon, Appl. Phys. Lett. 81 (2002) 4991.
[5] G.A. Medvedkin, T. Ishibashi, T. Nishi, K. Hayata, Y. Hasegawa, K. Sato, Jpn. J. Appl. Phys. 39 (2000) L949.
[6] K. Sato, G.A. Medvedkin, T. Nishi, Y. Hasegawa, R. Misawa, K. Hirose, T. Ishibashi, J. Appl. Phys. 89 (2001) 7027.
[7] S. Cho, S. Choi, G.-B. Cha, S.C. Hong, Y. Kim, Y.-J. Zhao, A.J. Freeman, J.B. Ketterson, B.J. Kim, Y.C. Kim, B.-C. Choi, Phys. Rev. Lett. 88 (2002) 257203.
[8] S. Cho, S. Choi, S.C. Hong, Y. Kim, J.B. Ketterson, B.J. Kim, Y.C. Kim, J.-H. Jung, Phys. Rev. B 66 (2002) 033303.
[9] G.A. Medvedkin, K. Hirose, T. Ishibashi, T. Nishi, V.G. Voevodin, K. Sato, J. Cryst. Growth 236 (2002) 609.

[10] Y.D. Park, A.T. Hanbicki, S.C. Erwin, C.S. Hellberg, J.M. Sullivan, J.E. Mattson, T.F. Ambrose, A. Wilson, G. Spanos, B.T. Jonker, Science 295 (2002) 651.
[11] M. Bolduc, C. Awo-Affouda, A. Stollenwerk, M.B. Huang, F.G. Ramos, G. Agnello, V.P. LaBella, Phys. Rev. B 71 (2005) 033302.
[12] F.M. Zhang, X.C. Liu, J. Gao, X.S. Wu, Y.W. Du, Appl. Phys. Lett. 85 (2004) 786.
[13] T. Dietl, H. Ohno, F. Matsukura, J. Cibert, D. Ferrand, Science 289 (2000) 1019.
[14] C.I. Harris, S. Savage, A. Konstantinov, M. Bakowski, P. Ericsson, Appl. Surf. Sci. 184 (2001) 393.
[15] P. Masri, Surf. Sci. Rep. 48 (2002) 1.
[16] N. Theodoropoulou, A.F. Hebard, S.N.G. Chu, M.E. Overberg, C.R. Abernathy, S.J. Pearton, R.G. Wilson, J.M. Zavada, Electrochem. Solid State Lett. 4 (2001) G119.
[17] N. Theodoropoulou, A.F. Hebard, S.N.G. Chu, M.E. Overberg, C.R. Abernathy, S.J. Pearton, R.G. Wilson, J.M. Zvada, Y.D. Park, J. Vac. Sci. Technol. A 20 (2002) 579.
[18] M.S. Miao, W.R.L. Lambrecht, Phys. Rev. B 68 (2003) 125204.
[19] L.B. Mccusker, R.B. Von Dreele, D.E. Cox, D. Louër, P. Scardi, J. Appl. Cryst. 32 (1999) 36.
[20] S.J. Pearton, Y.D. Park, C.R. Abernathy, M.E. Overberg, G.T. Thaler, J. Kim, F. Ren, J.M. Zavada, R.G. Wilson, Thin Solid Films 447–448 (2004) 493.
[21] J. Yang, W.H. Song, Y.Q. Ma, R.L. Zhang, B.C. Zhao, Z.G. Sheng, G.H. Zheng, J.M. Dai, Y.P. Sun, Phys. Rev. B 70 (2004) 144421.
[22] J.K. Furdyna, J. Appl. Phys. 64 (1988) R29.
[23] N.I. Medvedeva, E.I. Yur'eva, A.L. Ivanoskiĭ, Semiconductors 37 (2003) 1281.
[24] V.A. Gubanov, C. Boekema, C.Y. Fong, Appl. Phys. Lett. 78 (2001) 216.
[25] V.L. Shaposhnikov, N.A. Sobolev, J. Phys.:Condens. Matter 16 (2004) 1761.
[26] F. Beeler, O.K. Andersen, M. Scheffler, Phys. Rev. B 41 (1990) 1603.
[27] H. Akai, Phys. Rev. Lett. 81 (1998) 3002.
[28] S. Sanvito, P. Ordejo′n, N.A. Hill, Phys. Rev. B 63 (2001) 165206.
[29] Y.-J. Zhao, W.T. Geng, K.T. Park, A.J. Freeman, Phys. Rev. B 64 (2001) 035207.
[30] M. Jain, L. Kronik, J.R. Chelikowsky, Phys. Rev. B 64 (2001) 245205.
[31] T. Dietl, Semicond. Sci. Technol. 17 (2002) 377.
[32] R.N. Bhatt, X. Wan, M.P. Kennett, M. Berciu, Comput. Phys. Commun. 147 (2002) 684.
[33] D.P. Norton, S.J. Pearton, A.F. Hebard, N. Theodoropoulou, L.A. Boatner, R.G. Wilson, Appl. Phys. Lett. 82 (2003) 239.
[34] M. Yamada, T. Goto, T. Kanomata, J. Alloys Compd. 364 (2004) 37.
[35] J.J. Hauser, Phys. Rev. B 22 (1980) 2554.